degradation products was 2 amu, but common losses were of 18 (corresponding to water) and 116 (corresponds to 2,2-dimethyl butanoic acid). All the major degradation products were identified and characterized on the basis of their molecular ion peak and fragmentation behaviour. The major oxidative degradation products were found to be hydroxyl ketones and dihydroxy simvastatin, whereas diastereomers of hydroxy acid, drug and dehydrated lactone were formed under acidic conditions, as in the case of atorvastatin (Shah et al 2008).

Conclusions A stability-indicating assay method was developed and in total nine degradation products of simvastatin were characterized by LC-MS/TOF.

Shah, R. P. et al (2008) *Rapid Commun. Mass Spectrom.* **22**: 613–622

24

Molecular identification of St John's wort by PCR amplification of the ITS1 region: implications for medicinal plant identification

C. Howard, P. D. Bremner, M. R. Fowler and A. Slater

Department of Health and Life Sciences, De Montfort University, Leicester, UK.
E-mail: pbremner@dmu.ac.uk

Objectives The increase in use of medicinal plant products has highlighted the necessity for assurances of identification and quality in commercial products. We report the development of a DNA-based method for the identification and authentication of plant species, based upon the economically important St John's wort (SJW; *Hypericum perforatum* L.). Such methods can be applied to enhance the datasets (microscopic, chemical) required for the accurate identification of economically important medicinal plants. Medicinal plant products for human use in the European Union are regulated by the Traditional Herbal Medicines Directive.

Methods The ITS regions of the nuclear-encoded rRNA genes were the target for primer design. The ITS1 region is flanked on the 5′ and 3′ ends by the coding sequence of 18 and 5.8S rRNA, whereas ITS2 is flanked by 5.8 and 28S rRNA. The rRNA coding regions are highly conserved throughout plant species but the ITS sequences have an evolutionary rate which results in inter-species variation and intra-species conservation. PCR primers were designed for this variable region and specific primers, within this region, to selectively identify SJW. Nine species of vouchered DNA samples from the DNA Bank of the Royal Botanic Gardens, Kew, UK, were used as confirmed species specimens. These samples were used as a reference to ensure that the method could accurately discriminate SJW among six other *Hypericum* species grown from seed and garden-collected. Finally, three commercial medicinal products of or claiming to contain SJW were tested. PCR protocols were based upon the ITS1 region being successfully amplified in all DNA samples using primers ITS1 (5′-TCCGTAGGTGAACCTGCGG-3′) and ITS4 (5′-TCCTCCGCTTATTGATATGC-3′) (Crockett et al 2004). Further specific PCR primers were designed within the ITS region: FO2 (5′-CATAA-GAAGTGTAAGGCTCCCGG-3′), RO (5′-CGATACTTGGTGTGAATTGCA-GAA-3′) and HI-S (5′-CTCCTTCTGTTCATAACAATAACGACTCT-3′).

Results The FO2 and HI-S primers were designed to encompass the most divergent regions of the ITS1 sequence in the *Hypericum* species. This combined effect caused the primer pairing to give a specific PCR product with all three SJW samples. Of the nine *Hypericum* samples tested, a product with the primer pairing FO2 and HI-S was only found with SJW and *Hypericum delphicum*. This is expected due to the sequence similarity of this species at the FO2-binding site. However, this species is not widespread, and is unlikely to be found as a substitution or adulterant of SJW on sale commercially. Of the seven non-vouchered *Hypericum* samples tested, a product with this primer pairing also identified SJW as opposed to the other six samples. These results show that the primer combination can be used to differentiate non-vouchered samples from the economically valuable SJW. This same primer pairing also identified SJW in only two of three commercial products that listed SJW as an ingredient. DNA detection levels confirmed the PCR product from 0.00075 μg of DNA (0.1% genomic DNA).

Conclusions The method utilized in this study has enabled the design of a rapid and reliable molecular identification method for SJW. This has the potential to become a model for molecular identification design, and may be reproducible in other economically valuable plants.

Crockett, S.L. et al (2004) *Planta Medica* **70**: 929–935

Short Papers in Drug Delivery

25

The use of dendriplexes as a novel vaccine-delivery system against anthrax

S. J. Ribeiro[1,2], S. G. Rijpkema[3], Z. Durrani[3] and A. T. Florence[1]

[1]School of Pharmacy, London, [2]Abbott Laboratories, Queenborough and [3]National Institute for Biological Standards and Control, South Mimms, Potters Bar, UK.
E-mail: suzie.ribeiro@abbott.com

Objectives Two cationic polylysine dendron complexes with DNA (so-called dendriplexes) have been studied as the basis of a potential genetic anthrax vaccine. *Bacillus anthracis* has attracted attention as an agent for bioterrorism, calling for the development of new anthrax vaccines to protect humans against their intentional use. The virulence of anthrax bacilli is due to the production of a three-component protein exotoxin. Protective antigen (PA), one of the protein components, is singularly the most important antigen required for specific immunity to anthrax. The cationic dendrons have branched asymmetrical polylysine dendritic head groups attached to a head group, one with three C_{18} chains and the other without. Dendrons interact with and condense DNA, producing a complex with a small residual negative surface charge, and enhance cellular internalization of DNA, in part protecting the DNA from degradation.

Methods The dendrons (Figure 1) were synthesized by stepwise solid-phase peptide synthesis from Boc-Lys(Boc)-OH and 2-amino octadecanoic acid for C_{18} dendron and Boc-Ala-OH for C_0 dendron (Novabiochem) on 4-methyl benzhydrylamine resin using the Boc strategy (Sakthivel et al 1998). The C_0 dendron ($(C)_0(Lys)_7(NH_2)_8$) contains seven lysine groups and eight amino groups attached to the core and the C_{18} dendron ($((C_{18})_3(Lys)_7(NH_2)_8$) contains an additional three hydrocarbon chains. Two types of plasmid DNA were developed, one encoding PA 83 cloned into the eukaryotic expression plasmid pSecTag 2B (7.3 kbp) and a control plasmid without PA 83. The plasmids were complexed with dendrons, forming particles approximately 80 nm in size depending on the lipophilicity of the dendron. A/J and Balb/c mice were vaccinated with dendriplexes containing 1 and 50 μg plasmid DNA per dose over a period of 6 weeks.

Results Immunogenicity was determined using the enzyme-linked immunosorbent assay (ELISA) method for anti-PA antibodies. Naked PA immunization with multiple dosing did not induce a sufficient antibody response even after secondary boosting after primary intramuscular immunization, whereas both dendriplexes produced a strong anti-PA antibody response. The response was dose-dependent, as depicted by the low- and high-dose dendriplex treatment groups. Throughout the *in vivo* study both dendriplexes improved immunomodulatory efficiency in comparison with the naked PA DNA. However, the elicited antibodies did not neutralize lethal toxin *in vitro* (Ribeiro et al 2008).

Conclusions To our knowledge this is the first *in vivo* study using dendriplexes in a vaccine against anthrax. Further work is required to improve these preparations to elicit functional antibodies.

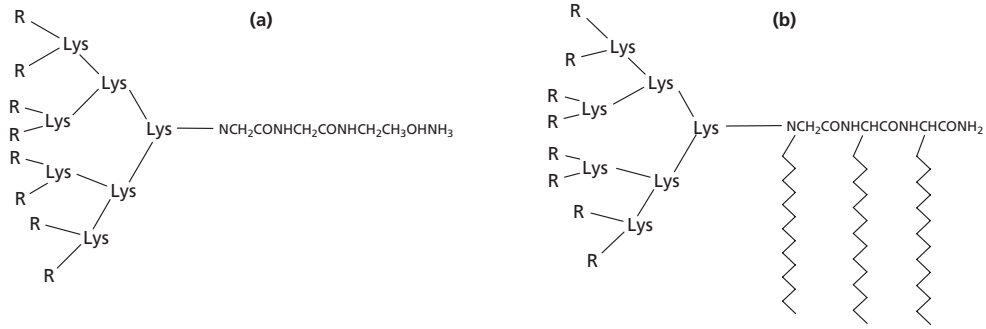

Figure 1 Simplified structure of the cationic lysine-based dendrons (a) C_0 ($(C)_0(Lys)_7(NH_2)_8$) with a molecular mass of 1174.91 Da and (b) C_{18} ($((C_{18})_3(Lys)_7(NH_2)_8$), of 1758.45 Da. Both dendrons contain 16 amino groups of which seven lysine groups (Lys) are attached to the core.

Ribeiro, S.J. et al (2008) *Open Vaccine* in press
Sakthivel, T. et al (1998) *Pharm. Res.* **15**: 776–782

26
Intravenous infusions of gentamicin in neonate patients: effects of infusion variables on drug administration rates

N. J. Medlicott[1], C. Sherwin[1], R. Broadbent[1,2], F. McCaffrey[2] and D. Reith[1,2]

[1]School of Pharmacy, University of Otago and [2]Otago District Health Board, Dunedin, New Zealand. E-mail: natalie.medlicott@otago.ac.nz

Objectives To investigate gentamicin infusion rates using typical neonate infusion protocols to quantify the drug input for pharmacokinetic studies.

Methods Intravenous infusions were set up to simulate administration of gentamicin to neonates. The intravenous line included an inline filter (0.2 μm, PALL medical filtration), a Baxter T-connector extension set, a BD connector plus 3, Medex Rem 160 3-way stopcock, a Baxter syringe T-piece Smart site luerlock and an Insyte IV catheter 22G. Dextrose 10% at flow rates of 3.8 and 18.7 mL/hour (Baxter neonatal pump) was used to reflect infusion rates for extremely low-birth-weight and term neonates respectively. A Graseby syringe driver was used to deliver gentamicin (0.5, 2.0, 2.5 or 10 mg) via the T-connection over 35 minutes followed by a 0.9% normal saline flush (1 or 2 mL) over 35 minutes. At the end of the infusion, a bolus of 2 mL of normal saline was administered to flush remaining drug from the line. Samples were collected over 75 minutes at 5 minute intervals from the end of the peripheral catheter. Gentamicin was derivatized with FMOC-Cl and measured by reverse-phase high-performance liquid chromatography (RP-HPLC) with fluorescence detection (internal standard was tobramycin). The assay was linear over the range 2–100 μg/mL for the C1, C1a, C2 and C2a components of gentamicin ($R^2 > 0.99$). Calibration curves for the C1a component were used for quantitation. Cumulative gentamicin delivered was determined and least squares linear regression analysis was used to fit a straight line to the infusion data (Stata®, version 9).

Results Gentamicin delivery was linear with respect to time over the infusion and saline flush (Figure 1). Dose delivered (%) in 60 and 75 minutes, rate of delivery (%/minute) and lag times (minutes), determined from linear regression, were compared using one-way analysis of variance. Infusions simulating delivery to neonates of more than 3.5 kg (10 mg gentamicin, dextrose flow rate 18.7 mL/minute) delivered 74.6 ± 2.2 and 80.2 ± 1.2% by 60 minutes and 86.0 ± 1.7 and 92.6 ± 1.2% by 75 minutes for 1 and 2 mL saline flushes respectively. Infusions for neonates of less than 3.5 kg (2 mg gentamicin, dextrose flow rate 3.8 mL/hour, saline flush 1 mL) showed 61.1 ± 1.9 and 74.9 ± 1.9% gentamicin delivered by 60 and 75 minutes respectively. Recovery of the dose was less for a lower gentamicin dose (61.7 ± 4.3% at 60 minutes for a 0.5 mg dose) but increased when saline flush volume or dextrose flow rate was increased.

Conclusions Infusion parameters affected both the gentamicin dose recovery and rate of delivery from neonatal infusions and have implications for pharmacokinetic studies and interpretation of peak concentrations in these patients.

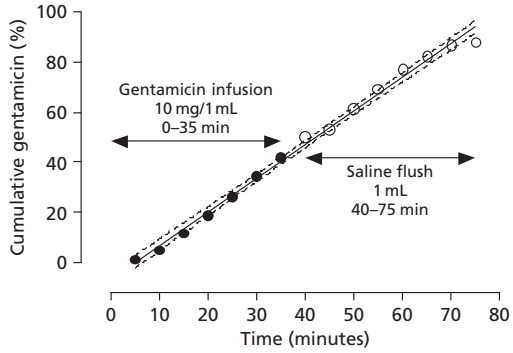

Figure 1 Cumulative gentamicin delivered for a 10 mg dose delivered into 10% dextrose (18.7 mL/hour), saline flush 1 mL over 35 minutes ($R^2 > 0.99$).

27
Overcoming the mucin barrier in the treatment of pulmonary cystic fibrosis

G. A. Hutcheon, E. Gaskell, A. Iftikhar and C. Rostron

School of Pharmacy and Chemistry, Liverpool John Moores University, Liverpool, UK. E-mail: G.A.Hutcheon@ljmu.ac.uk

Objectives The objective of this research is to improve the delivery of therapeutic agents to cystic fibrosis (CF) patients by overcoming the mucus barrier that challenges current pulmonary therapies. Mucoregulators such as *N*-acetylcysteine, recombinant human DNase and hypertonic saline are currently used to decrease the viscosity of inspissated mucus as separate treatments to the anti-microbial and anti-inflammatory therapeutic agents. This work outlines progress in developing a combined drug-delivery system bringing together the mucinolytic abilities of microbially produced proteases and an anti-inflammatory drug.

Methods Biodegradable polyester-co-lactones were enzymatically synthesized as described previously (Namekawa et al 2000). Microparticles were prepared via single and multiple emulsion-solvent evaporation (Gaskell et al 2008) and visualized by scanning electron microscopy. Ibuprofen was encapsulated as a model drug and α-chymotrypsin as a model enzyme. The α-chymotrypsin encapsulation efficiencies were monitored via quantitative spectrophotometric and protease activity assays (azocasein assay and MUTMAC active-site titration). Ibuprofen encapsulation was quantified using high-performance liquid chromatography and UV spectroscopy. Subsequent release of both components from the polymeric particles was monitored *in vitro*. The released enzyme was assayed for activity as outlined above. Cytotoxicity studies of the polymeric delivery systems were undertaken using standard 3-(4,5-dimethylthiazol-2-yl)-2,5-diphenyl-2*H*-tetrazolium bromide (MTT) tests.

Results A family of polyester-co-lactones with and without pendant hydroxyl groups was synthesized and used to encapsulate α-chymotrypsin and/or ibuprofen. By varying the process parameters, particles within the size range of 1–5 μm were formulated. Enzyme encapsulation was achieved up to 10% with maximal release being achieved upon 2–3 hours. The activity of the released enzyme deteriorated after an hour, regardless of the particle preparation conditions used. Up to 20% ibuprofen was encapsulated; however, a burst release was evident with maximal release in the first hour. The polymer chemistry was shown to have an effect on particle morphology, encapsulation and release of the active agents considered. These particles exhibited low cytotoxicity, indicating that they are good candidates for targeted drug-delivery systems.

Conclusions These materials have shown potential for further development with the possibility of altering the chemistry of the polymer to meet the requirements of a specific delivery system. The burst release of ibuprofen may be overcome by covalent attachment of the drug to the polymer backbone (Thompson et al 2008), thus obtaining sustained release. A range of microbially produced serine and metalloproteases have been identified as prominent mucin-degrading enzymes and are currently being investigated as potential candidates for targeted mucin degradation. In the future, an *in vitro* model is required to assess the effectiveness of such a combined delivery system in overcoming the mucus barrier and aiding the delivery of the target drug.

Gaskell, E. E. et al (2008) *J. Microencapsul.* in press
Namekawa, S. et al (2000) *Biomacromol.* **1**: 335–338
Thompson, C. J. et al (2008) *Drug Dev. Ind. Pharm.* in press

28
Controlled delivery of doxorubicin and rapamycin from embolization microspheres to treat hepatocellular carcinoma

R. E. J. Forster[1,2], C. Bowyer[1], A. L. Lewis[2], W. M. Macfarlane[1], G. J. Phillips[1] and A. W. Lloyd[1]

[1]University of Brighton, Brighton and [2]Biocompatibles UK, Farnham, UK. E-mail: richard.forster@biocompatibles.com

Objectives Transarterial chemoembolization (TACE) is a technique used to treat unresectable liver cancer that is becoming a clinical norm (Golzarian et al 2006). The technique has been further refined by use of sulphonate-modified polyvinyl alcohol drug-eluting beads (DEBs; DC Bead™) that can be loaded with doxorubicin, allowing a controlled, sustained and localized release of the drug directly to the tumour (Lewis et al 2007). The aim of this study was to determine whether the simultaneous and/or sequential release of rapamycin and doxorubicin during DEB-TACE could provide a more effective treatment by investigating the survival/proliferation of HepG2 cells exposed to both drugs under normoxic conditions. Subsequently the study will be repeated using a hypoxic HepG2 cell model.

Methods Rapamycin loading involved swelling the DEBs (1 mL) in dimethylsulphoxide (DMSO) and adding rapamycin solution (DMSO, 1 mL; 60 mg/mL). Excess rapamycin solution was removed and the remaining slurry washed with water. Doxorubicin loading was achieved by immersing the unloaded DEBs into a doxorubicin solution (water, 2 mL; 18.75 mg/mL) and agitating for 60 minutes. When loaded in combination, rapamycin was loaded first. Total loading was determined by extracting the drug from the DEBs (using DMSO) and analysed using UV-visible spectroscopy (with reference to standard solutions). The elution profiles of rapamycin and doxorubicin from DEBs into 200 mL phosphate-buffered saline (PBS) were determined using UV-visible spectroscopy (using standard solutions). The elution media (5 mL) were extracted at various time points for analysis and replaced with 5 mL fresh PBS. The cytotoxicity of the drug-loaded beads towards normoxic HepG2 cells was assessed using

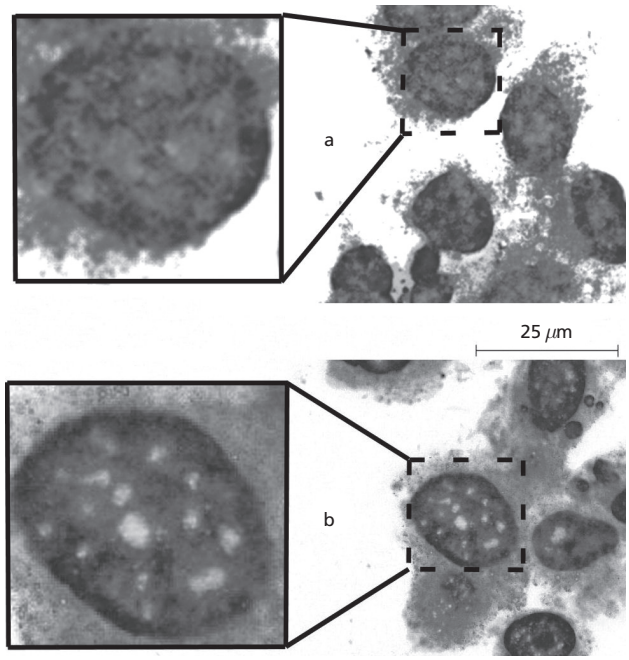

Figure 1 Inhibition (a) and activation (b) of NF-κB by rapamycin and doxorubicin respectively.

3-(4,5-dimethylthiazol-2-yl)-5-(3-carboxymethoxyphenyl)-2-(4-sulfonphenyl)-2H-tetrazolium (MTS) assays at selected time points and any synergistic effects were quantified using the combination index equation. Nuclear factor κB (NF-κB) activation was monitored using confocal microscopy and immunohistochemical staining.

Results The loading (per millilitre of DEBs) was 35.5 mg of doxorubicin and 20 mg of rapamycin for individually and dual-loaded DEBs. The elution profiles were similar ($f_1 < 15$ and $f_2 > 50$ by US Food and Drug Administration (FDA) elution test (BP1)) under the *in vitro* conditions used (note: the elution profile is not fully representative of drug elution *in vivo*). The cytotoxicity of drug combinations from the dual-loaded beads compared with two individually loaded beads showed no significant difference ($P > 0.05$): 38% (24 hours), 7% (48 hours) and 0.8% (72 hours). Rapamycin and doxorubicin combinations displayed a strongly synergistic effect (cell viability after 72 hours: rapamycin 62%; doxorubicin 6%; both 0.8%; combination index < 0.1). NF-κB was shown by immunohistochemical staining to undergo greater activation from doxorubicin than rapamycin (Figure 1). This activation was reduced when rapamycin and doxorubicin were used in combination.

Conclusions The presence of rapamycin and doxorubicin in the same DEB did not significantly affect the loading or elution properties of each other. The delivery of combinations from the DC Bead™ potentially offers the benefits of embolization, localized drug delivery and combination drug therapy within a single technique. Analysis of this novel drug-delivery method utilizing our recently developed hypoxic model system, confirmed through the upregulation of hypoxia-inducible factor 1a (HIF-1a) and vascular endothelial growth factor (VEGF) using sodium dodecyl sulphate (SDS)/polyacrylamide-gel electrophoresis (PAGE) and western-blot analysis, may provide new insights into effective treatments for hepatocellular carcinoma.

Golzarian, J. et al (2006) *Vascular embolotherapy*. Springer
Lewis, A. et al (2007) *J. Mater. Sci. Mater. Med.* **18**(9): 1691–1699

29
Developing novel temperature-responsive polymers for drug delivery

V. V. Khutoryanskiy[1] and G. A. Mun[2]

[1]School of Pharmacy, University of Reading, Reading, UK and [2]Department of Chemical Physics and Macromolecular Chemistry, Kazakh National University, Almaty, Kazakhstan. E-mail: v.khutoryanskiy@reading.ac.uk

Objectives Temperature-responsive water-soluble polymers may be used for developing *in situ* gelling systems for drug delivery. In aqueous solutions these systems are able to undergo a transition from liquid at relatively low temperatures (5–10°C) to a semisolid gel upon exposure to the physiological environment (35–37°C). The objective of the present work was to develop a range of novel water-soluble polymers that exhibit temperature-responsive properties, to study the influence of different factors affecting their temperature-induced phase transitions and to evaluate the possibility of their application for formulating *in situ* gelling drug-delivery systems.

Figure 1 Solution of a temperature-responsive polymer below (a) and above (b) the temperature of phase separation (TPS).

Methods A series of copolymers were synthesized by copolymerizing monomers of a hydrophilic nature (2-hydroxyethyl acrylate and *N*-vinyl pyrrolidone) with monomers of relatively hydrophobic nature (butyl vinyl ether, propyl vinyl ether and 2-hydroxyethyl methacrylate). The behaviour of the copolymers in solution was studied by dynamic light scattering at different temperatures. The ability of selected copolymers to form micellar structures was assessed by fluorescence spectroscopy with pyrene as a probe and by transmission electron microscopy.

Results The solubility of the copolymers in water depends on the nature and the content of a hydrophobic monomer. These water-soluble copolymers exhibit temperature-responsive properties; that is, they undergo phase separation upon increase in temperature. At relatively low concentrations of the copolymer (1–20 mg/mL) the phase separation results in formation of colloidal solutions (Figure 1). The temperature of phase separation (TPS) depends on a number of factors including the composition of copolymers, their chemical nature and the concentration in solution. An increase in the content of relatively hydrophobic monomer in copolymers results in decrease of TPS, which is attributed to their stronger ability to aggregate. An incorporation of the copolymers with longer alkyl chain into the structure of copolymers also reduces their TPS. The TPS may also be altered by adding inorganic salts, urea or ethanol.

Conclusions A range of novel temperature-responsive water-soluble copolymers can be synthesized by copolymerizing monomers of a hydrophobic nature with monomers of a hydrophilic nature. These copolymers are promising candidates for developing *in situ* gelling systems for drug delivery.

30
Incorporation of acetazolamide into niosomes using a novel pH gradient technique: a characterization study

A. Vangala[1] and S. Rasul[2]

[1]Department of Pharmacy and Chemistry, Kingston University, Kingston-upon-Thames and [2]Aston University, Birmingham, UK. E-mail: A.Vangala@kingston.ac.uk

Objectives Glaucoma is an ophthalmic condition that leads to a rise in intraocular pressure (IOP). The carbonic anhydrase inhibitor acetazolamide (ACZ), administered to reduce IOP, induces systemic side effects such as metabolic acidosis. Previous attempts to administer the drug topically have failed, possibly due to low aqueous solubility and corneal residence time of the drug. Niosomes (non-ionic surfactant vesicles) have been shown to increase drug concentration at the ocular site and minimize side effects (Aggarwal and Kaur 2005). Incorporation of ACZ into niosomes using a novel pH gradient entrapment technique and the physico-chemical characterization of these systems were carried out as part of the present work.

Methods Multilamellar vesicles (MLVs) and small unilamellar vesicles (SUVs) composed of Span 60 and cholesterol (1:1 molar ratio) with or without chitosan (0.2% v/v), encapsulating ACZ, were prepared by film-hydration method. Niosomes were preloaded with boric acid solution to lower the internal pH of the vesicle's

aqueous core (≈ pH 5.0). The acidified niosomes were then incubated in a solution of sodium salt of ACZ at pH 9.0. The permeability of the vesicles was raised by increasing the temperature of the medium above the phase-transition temperature (T_c) of Span 60. The water-soluble sodium form of ACZ was then permeated through the niosomal membrane into the acidic core where it would be converted to ACZ-free acid (sulphonamide), which is insoluble and would be entrapped within the niosomes. Vesicle sizes and zeta potential were measured on a Brookhaven instrument. Drug-release studies were conducted using dialysis membrane.

Results Results showed that entrapment values of MLV-ACZ, SUV-ACZ and chitosan-coated SUV-ACZ niosomes were 84.0 ± 1.5, 97.5 ± 1.1 and 98.0 ± 1.3% respectively, showing that the chitosan coat on the SUV-ACZ preparations made no significant difference ($P < 0.05$) in drug loading. The vesicle sizes of drug-loaded SUVs in the presence or absence of the chitosan coat were 455.8 ± 2.3 and 416.8 ± 3.5 nm respectively. The zeta potential of drug-loaded, uncoated SUV was –41.4 ± 3.0 as opposed to its coated counterpart (51.6 ± 1.9), suggesting the formation of a stable coat over the vesicle surface and resulting in the shift of surface charge from a negative to a positive value. In the release studies conducted for 24 hours at 25°C, ACZ release from MLVs, SUVs and chitosan-coated SUV were 37.9 ± 0.4, 43.0 ± 0.8 and 27.8 ± 0.7% respectively. 'Empty' niosomes were stable for 21 days at room temperature whereas the stability data of the drug containing and 'empty' niosomes showed a significant increase in vesicle size (from 380.4 ± 7.5 to 559.2 ± 2.8 nm) at 37°C, showing no significant change in zeta potential over 15 days.

Conclusions These studies demonstrate the effectiveness of the novel pH gradient entrapment technique with which drug loading into the niosomes was carried out. Ocular availability of ACZ could be improved with a high payload and sustained drug release with chitosan coat, a non-irritant to the eye. However, further work in reducing niosome sizes to improve the compliance of the preparation is currently under progress.

Aggarwal, D., Kaur, P. I. (2005) *Int. J. Pharm.* **290**: 155–159

31
Effect of nano-hydroxyapatite on controlled release of leuprolide acetate from *in situ*-forming PLGA implant

M. Enayati[1], H. Mobedi[2] and H. Mirzadeh[1,2]

[1]Department of Biomedical Engineering, Amirkbair University of Technology and [2]Iran Polymer and Petrochemical Institute, Tehran, Islamic Republic of Iran.
E-mail: marjan@enayati.ir

Objectives To reduce the burst release of leuprolide acetate drug in the first 24 hours from conventional *in situ*-forming biodegradable poly(D,L-lactide-*co*-glycolide) (PLGA) implant, the effect of nano-hydroxyapatite as an additive to this implant was studied.

Methods For preparation of 45:55 (w/w) RG752/*N*-methyl-2-pyrrolidone (NMP) and 30:70 (w/w) RG756/NMP solutions, appropriate amounts of PLGA 75:25 (Resomer® RG752H, 11700 Da, inherent viscosity = 0.18 dl/g; Resomer® RG756S, 81900 Da, inherent viscosity = 0.54) are dissolved in NMP as a solvent. The solutions are irradiated by gamma radiation at a dose of 25 kGy. Two types of formulation were prepared as the implant's base: RG756 and RG756/RG752, 3:1. The drug luprolide acetate, 6% (w/w), was loaded in these implants. The burst release of the two implants was studied under three conditions: (1) without any hydroxyapatite additive, (2) with 5% (w/w) nano-hydroxyapatite powder additive and (3) with 10% (w/w) nano-hydroxyapatite powder additive. Nano-hydroxyapatite powders were prepared by precipitation from supersaturated aqueous solutions using analytical-grade reagents. The characterized nano-hydroxyapatite powders had an atomic ratio of 1.7 and particle size of 54 nm. Each formulation (0.5 g) was injected into 10 mL of phosphate buffer (0.2 M, pH 7.4). The concentration of released leuprolide acetate was determined by high-performance liquid chromatography (HPLC). Surface and interior morphologies of implants after various predetermined durations of incubation were also studied by scanning electron microscopy.

Results Nano-hydroxyapatite powder caused an initial reduction in leuprolide acetate burst release: 5 and 10% nano-hydroxyapatite decreased burst release to 6 and 8% in RG756 implants and 7 and 8% in RG756/RG752, 3:1, implants respectively. Solvent dissipation and water penetration through the implant decreased in the presence of nano-hydroxyapatite. As a result, phase separation, phase inversion and polymer precipitation occurred at lower rates. This led to a more compact and less porous structure with fewer interconnected channels (Figure 1). Due to this spongy and compact structure, a smaller burst release and more sustained drug release was achieved.

Conclusions Implant containing nano-hydroxyapatite additive had a smaller initial burst with more sustained drug release. Nano-hydroxyapatite particles reduced the pores and interconnected channels and made the structure of the implant more compact and spongy.

32
Investigation of swelling and network parameters of poly(ethylene glycol)-crosslinked poly(methyl vinyl ether-*co*-maleic anhydride) hydrogels

T. R. R. Singh, R. F. Donnelly, P. A. McCarron, D. A. Woolfson and D. I. J. Morrow

School of Pharmacy, Queen's University, Belfast, UK. E-mail: rthakur01@qub.ac.uk

Objectives Hydrogels are three-dimensional, hydrophilic, polymeric networks capable of imbibing large amounts of water or biological fluids. In the present study we investigated swelling of hydrogels of poly(methyl vinyl ether-*co*-maleic anhydride) (PMVE/MA) crosslinked with different molecular weights (10000, 1000 and 200 Da) of poly(ethylene glycol) (PEG). In addition, the molecular interactions between PMVE/MA and PEG were investigated using attenuated total reflectance (ATR)-Fourier transform infrared (FTIR) spectroscopy and nuclear magnetic resonance (NMR). The goal of this research was to develop hydrogels for controlled drug delivery.

Methods A total of 18 films were prepared by casting of aqueous gels containing PMVE/MA at 10, 15 and 20% w/w in 2:1 and 4:3 ratios with each of the PEGs. Films were crosslinked for 24 hours at 80°C. Crosslinked films (1 cm^2) were cut from each xerogel and swollen in deionized water for 7 days and weighed at regular intervals. Network parameters, such as equilibrium water content (EWC), molecular weight between crosslinks (M_c), polymer–solvent interaction parameter (χ), crosslink density (q) and polymer volume fraction (ϕ), were determined by mathematical treatment of swelling results. In addition, crosslinked films were tested in ATR-FTIR and NMR studies for determination of the nature of crosslinks.

Results PMVE/MA hydrogels crosslinked with PEG 10000 showed the highest percentage of swelling, followed by PEG 1000 and PEG 200 films. In general, the crosslinking density of the films was increased with a decrease in the molecular weight and increase in concentration of PEG. Table 1 shows the network parameter results of a 2:1 ratio of PMVE/MA at 20% w/w and PEG hydrogels.

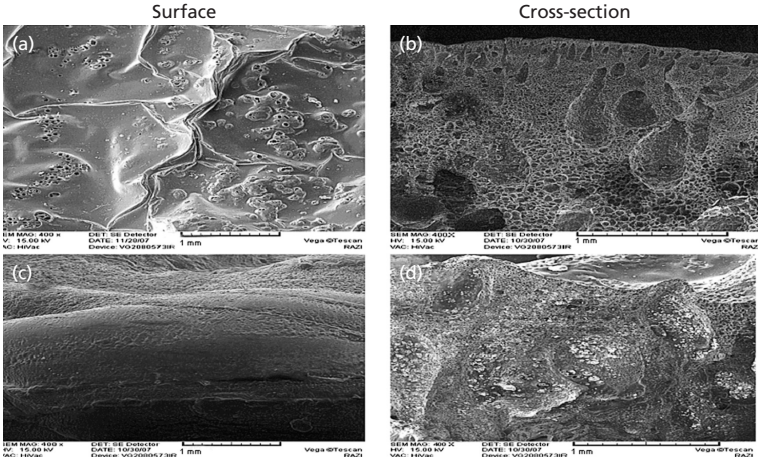

Figure 1 Morphology of RG756 3 days after incubation: (a, b) implant without nano-hydroxyapatite; (c, d) implant with 5% nano-hydroxyapatite.

Table 1 Network parameters of 2:1 ratio of 20% PMVE/MA and PEG (10000, 1000 and 200 Da) crosslinked hydrogels

Network Parameters	PMVE/MA:/PEG, 2:1		
	10000	1000	200
EWC (%)	78.57	58.90	39.47
M_c **(g/mol)**	1203.15	980.63	453.33
χ	0.7313	0.7880	0.8121
q	0.1446	0.1774	0.3838
ϕ	0.69	0.86	0.94

Furthermore, NMR and ATR-FTIR studies showed the presence of peaks in the ester region, suggesting that etherification occurs between PMVE/MA and PEGs.

Conclusions NMR and ATR-FTIR studies showed the presence of ester linkage between PMVE/MA and PEGs. Hydrogels of PMVE/MA crosslinked with PEG 10000 showed a significantly higher degree of swelling, followed by PEG 1000 and PEG 200 crosslinked hydrogels. Therefore, PMVE/MA–PEG 10000 hydrogels could possibly be used for rapid delivery of drugs, due to their low crosslink density. In addition, moderately crosslinked PEG 1000 or highly crosslinked PEG 200 hydrogels could be used in controlling drug-delivery rates.

New Scientist Session "Pharmaceutical Sciences: Where are We Going?"

33
Intelligent anti-infective biomaterials

A. J. Croskery, G. A. Andrews, B. F. Gilmore, D. S. Jones and S. P. Gorman

School of Pharmacy, Queen's University, Belfast, UK.
E-mail: andrew.croskery@btinternet.com

Objectives One of the predominant problems with the use of urinary medical devices is the development of device infection: beginning with bacterial adherence, developing with the formation of biofilm and with the symptomatic end point of encrustation. Catheter encrustation can cause pain upon removal and increases the frequency with which catheters must be removed; this is particularly problematic for patients requiring long-term catheterization. Serious consequences include septicaemia, pyelonephritis and shock (Lawrence and Turner 2005). Approaches to overcoming this problem include the incorporation of antibiotics into the device to combat infection and also the modification of the device surface so that it is not as susceptible to infection. This work attempts to join these two approaches together in a synergistic manner, with a device surface that is inherently resistant to infection through intelligent *in vivo* reactions and which is also impregnated with antibiotics.

Methods Polymers were mixed with suitable plasticizers to enable processing with a twin-screw extruder. Different drug loadings of different anti-bacterial agents were then mixed with the polymer/plasticizer formulations. Formulations were stored in a desiccator for 24 hours prior to processing. The formulations were then extruded with varying concentrations of anti-bacterial agent. The samples were suspended in release medium appropriate to the *in vivo* conditions. Samples were then filtered using 0.45 μm syringe filters and analysed using UV spectroscopy to determine their drug-release properties.

Results The different polymers demonstrated an intelligent response, with one polymer demonstrating drug release in conditions mimicking infection, and the other demonstrating drug release in conditions mimicking both the healthy state and an infected device.

Conclusions These polymers are suitable for further investigation as a novel responsive anti-infective medical-device coating, providing actions to both prevent and treat medical-device infection.

Lawrence, E. L., Turner, I. G. (2005) *Med. Eng. Phys.* **27**: 443–453

34
Novel approaches to characterizing phase separation and drug distribution across hot-melt-extruded solid dispersions containing poorly water-soluble drugs

S. Qi[1], J. Moffat[1], A. Gryczke[2], K. Nollenberger[2], P. Belton[1], M. Reading[1] and D. Craig[1]

[1]School of Chemical Sciences and Pharmacy, University of East Anglia, Norwich, UK and [2]Evonik Röhm GmbH, Evonik Industries, Darmstadt, Germany.
E-mail: sheng.qi@uea.ac.uk

Objectives To investigate the phase-separation behaviour of hot-melt-extruded (HME) solid dispersion formulations containing a poorly water-soluble drug. Novel approaches are introduced to characterize the phase-separation behaviour and map the drug distribution in the HME formulations at a micrometre to sub-micrometre scale of resolution. These approaches include local thermal analysis (LTA) using nano-thermal tips, photothermal microspectroscopy (PT-MS) and Fourier-transform infrared (FTIR) photoacoustic spectroscopy (PAS).

Methods Felodipine was incorporated into EUDRAGIT® E matrices using hot-melt extrusion. The drug/polymer ratios of the HME formulations were between 10/90 and 70/30. Pulsed-force mode atomic force microscopy (PFM-AFM) was performed to identify phase separation in the formulations. After the PFM-AFM imaging, LTA measurements were carried out at selected locations to further identify the thermal properties of each sampling point. PT-MS measurements were carried out by interfacing an FTIR spectrometer with an AFM equipped with a Wollaston probe; these experiments were performed at different locations across the surface and the cross-section of the HME strands. The photoacoustic spectra were taken using a Bruker IFS 66/S spectrometer fitted with a photoacoustic cell. The PAS spectral depth profiling of the HME samples was obtained using step scans at different frequencies.

Results The PFM-AFM imaging revealed phase separation in the solid dispersion of miscible felodipine and EUDRAGIT® E after hot-melt extrusion. Particles could be seen in the HME formulations with drug/polymer ratios at and above 30/70. The LTA measurements performed on the particles and the surrounding areas indicated the presence of different phases in the HME formulations. The thermal behaviour of these separated phases varied with the drug/polymer ratio of the HME solid dispersion. The PT-MS results demonstrated the differences in the drug concentration and distribution on the surface and at the cross-section of the HME strands with drug/polymer ratios at and above 30/70. To further investigate the depth profile of the drug distribution of the HME formulations, photoacoustic step-scan measurements were performed. Three different frequencies were applied in the step-scan measurements to allow the evaluation of the drug distribution at three different layers in depth from the surface of the HME strands. Combining these results with the PT-MS and conventional attenuated total reflectance (ATR)-FTIR results, the drug distribution of the formulations with phase separation was mapped on a micrometre scale.

Conclusions In this study, phase separation was observed in a miscible drug/polymer system after being processed using hot-melt extrusion. The presence of phase separation which varied with the drug/polymer ratio in the formulations was identified using PFM-AFM in conjunction with LTA analysis. The drug distribution across the HME solid-dispersion strands was characterized using PT-MS combined with conventional ATR-FTIR and PAS. The detailed depth profiles of the drug concentration at different layers of the HME formulations were obtained on a micrometre scale. These approaches are considered to represent a promising new approach to studying phase separation, particularly as the drug distribution within the HME strands may potentially affect the drug-release behaviour.

35
Preparation and characterization of glibenclamide microcrystals

A. Jatto and A. A. Elkordy

Department of Pharmaceutics, Sunderland School of Pharmacy, University of Sunderland, Sunderland, UK. E-mail: amal.elkordy@sunderland.ac.uk

Objectives Dissolution rate of hydrophobic drugs is the rate-limiting step for drug absorption. Increasing the specific surface area of the drug (by micronization) will lead to increasing the drug dissolution rate (Noyes–Whitney equation). Accordingly, glibenclamide, a model hydrophobic drug, was microcrystallized by *in situ* micronization method. The aim was to prepare glibenclamide microcrystals for oral delivery.

Methods A solvent change method was utilized to prepare drug microcrystals. In this method, Solutol-HS15 and Cremophor-RH40 (non-ionic surfactants) were used as stabilizers to control the size of precipitating crystals. Glibenclamide was dissolved in dichloromethane (0.2% w/v). Surfactants were dissolved in water in concentrations of 1, 2 and 5% w/v. Drug solution (10 mL) was mixed with surfactant solution (40 mL) by magnetic stirrer. Accordingly, microcrystals were formed spontaneously. The mixtures were centrifuged at 10000 rpm for 5 minutes and the precipitated crystals were freeze-dried via VirTis freeze drier. The dried glibenclamide microcrystals were characterized for particle size analysis (via Zeta Sizer), microcrystal morphology using scanning electron microscopy (SEM), drug solubility, drug dissolution using capsules containing 5 mg drug and structural analysis via Fourier-transform infrared (FTIR) spectroscopy.

Results Glibenclamide microcrystals produced a higher solubility ($P < 0.05$, analysis of variance) compared with that of commercial glibenclamide. This may be explained by large surface area and good wetting properties of drug microcrystals. The release of the drug from microcrystals was significantly higher ($P < 0.05$, analysis of variance) than that of commercial drug. After 5 minutes, the average percentages of drug release were 80% from microcrystals prepared with